Satellite detection of the convection generated stresses in Earth

Han-Shou Liu[1], Ronald Kolenkiewicz[1], Jinling Li[2], and Jizhong Chen[3]
1. NASA Goddard Space Flight Center, Greenbelt, MD 20771, USA
2. Astronomical Observatory, National Academy of Science, Shanghai, China
3. Sigma Space Corporation, Lanham, MD 20706, USA

April 1, 2003

POPULAR SUMMARY

We review research developments on satellite detection of the convection generated stresses in the Earth for seismic hazard assessment and Earth resource survey. Particular emphasis is laid upon recent progress and results of stress calculations from which the origin and evolution of the tectonic features on Earth's surface can be scientifically addressed.

An important aspect of the recent research development in tectonic stresses relative to earthquakes is the implications for earthquake forecasting and prediction. We have demonstrated that earthquakes occur on the ring of fire around the Pacific in response to the tectonic stresses induced by mantle convection. We propose a systematic global assessment of the seismic hazard based on variations of tectonic stresses in the Earth as observed by satellites. This space geodynamic approach for assessing the seismic hazard is unique in that it can pinpoint the triggering stresses for large earthquakes without ambiguities of geological structures, fault geometries, and other tectonic properties. Also, it is distinct from the probabilistic seismic hazard assessment models in the literature, which are based only on extrapolations of available earthquake data.

Satellite detection of convection-generated stresses in the interior of the Earth has a history in space and Earth sciences. It has been one of the most impressive and important Earth research program~~s~~ since the beginning of the space age. This program is applicable for identification of the forcing mechanisms for uplift, depression, rifting, volcanism, seismicity, plate motion, kimberlite magmatism, ore formation, and hot spots distribution on the surface of the Earth. It is shown that distribution of the 450 principal metal deposits in Africa is restricted in the tensional stress system and all ore deposits are clustered in areas of the uplifted old rocks, indicating that metal deposits of all ages in Africa were exposed by stress induced uplift. Most importantly, we have demonstrated that the intensive compressional and tensional stresses in the global stress concentration belts are the triggering stresses for the 131 $M_s \geq 7.0$ earthquakes for 1977 to 2000. Therefore, we conclude that recent research development in this special field of geophysics has provided a direct approach to seismic hazard assessment and Earth resources survey.

This paper is dedicated to the memory of S. Chandrasekhar, J. A. O'Keefe and S. K. Runcorn who saw that it must be true. We thank F. G. Lemoine and his research team members for providing satellite gravity data for our research development.

Satellite detection of the convection generated stresses in Earth

Han-Shou Liu[1], Ronald Kolenkiewicz[1], Jinling Li[2], and Jizhong Chen[3]
1. NASA Goddard Space Flight Center, Greenbelt, MD 20771, USA
2. Astronomical Observatory, National Academy of Science, Shanghai, China
3. Sigma Space Corporation, Lanham, MD 20706, USA

Short title: Satellite detection of stresses in Earth

ABSTRACT

We review research developments on satellite detection of the convection generated stresses in the Earth for seismic hazard assessment and Earth resource survey. Particular emphasis is laid upon recent progress and results of stress calculations from which the origin and evolution of the tectonic features on Earth's surface can be scientifically addressed.

An important aspect of the recent research development in tectonic stresses relative to earthquakes is the implications for earthquake forecasting and prediction. We have demonstrated that earthquakes occur on the ring of fire around the Pacific in response to the tectonic stresses induced by mantle convection. We propose a systematic global assessment of the seismic hazard based on variations of tectonic stresses in the Earth as observed by satellites. This space geodynamic approach for assessing the seismic hazard is unique in that it can pinpoint the triggering stresses for large earthquakes without ambiguities of geological structures, fault geometries, and other tectonic properties. Also, it is distinct from the probabilistic seismic hazard assessment models in the literature, which are based only on extrapolations of available earthquake data.

1. INTRODUCTION

O'Keefe [1] tested the basic hypothesis of geodesy using the harmonics of the Earth's gravity field from satellite measurements. He pointed out that these harmonics may be supported by hydrodynamic forces resulting from mantle convection. Runcorn [2, 3] developed a theory connecting mantle convection and the geoid. His calculations demonstrated that a large-scale flow system in the mantle corresponding to the low-degree harmonics of the geopotential has two features in accord with the paleomagnetic data: The separation of the Americas from Europe and Africa and the northward movement of India and Australia. Since heat source contents and viscosities yield short wavelength mantle flow in convection models [4], the higher degree harmonics of the geopotential may reflect the small-scale flow in the mantle convection system [5].

Although numerical calculations of thermal convection models of the mantle have been carried out by Turcotte and Oxburgh [6], McKenzie et al. [7] and Schubert et al. [8], the non-linear nature of mantle convection and the wide range of viscosities present formidable obstacles to the thorough knowledge of convection patterns. It may well be that unless simple models of mantle flow are first understood, complex cases would not be interpretable in terms of the contribution to geodynamics. Therefore, it seems necessary to apply the relative simple but realistic models of mantle convection for detection of tectonic forces or stresses using the harmonics of the Earth's gravity field.

By utilizing the satellite measurements of the Earth's gravity field, Liu [9, 10] has shown that the tensional, compressional and shear stress under the crust caused by mantle flows are of the order of 10^8 dyne cm^{-2}. Under appropriate configurations, the strains to be expected may be localized in fractures of the lithospheric shell and in some cases may lead to crustal deformation. We may conjecture that the rock of the mantle, the deep plastic region below the elastic rust, must be churning in convection cells to cause stress concentrations under the crust.

The fundamental problem of the deformation of the Earth involves stress condition on the base of the crust caused by mantle convection. Jeffreys [11], Runcorn, [3], and Hide and Horai [12] have done a spherical harmonic analysis of convention flow in the interior of the Earth. In a series of papers, Liu [9, 10, 13-26], has demonstrated that a certain band of the high degree harmonics of satellite gravity data is related to the subcrustal stresses under Asia, Africa, Australia, Europe, and North and South America. Also, Liu has calculated the stresses in the crust by applying the theory of shells and plates with subcrustal stresses as boundary conditions. The resultant calculated tensional, compressional, and shear stress regimes as inferred from satellite gravity data have provided an unified forcing mechanism for formation of the tectonic features on the surface of the Earth. Specifically, analysis of the subcrustal stress patterns as inferred from satellite gravity data has explained the origin of three earthquakes during the past three decades. [14, 18, 25].

The successively higher degree harmonics, which have been placed in the model of the Earth's gravity field, is one of the most impressive series of measurements in the space program. The developments of the GEM series of satellite gravity harmonics are accurate up from degree 2 to 25 in which the harmonics above degree 13 are related to the subcrustal stress field [14]. Now we have entered a new era in satellite measurements of gravity anomalies. The new Earth Gravitational Model 1996 (EGM96) has developed an improved spherical harmonics of the Earth's gravitational potential to degree and order of 360 [27]. Introducing the high degree harmonics coefficients of the gravity data for $13 \leq n \leq 150$ into the stress equations, we have obtained a global stress pattern which can be applied to seismic hazard assessment. The 131 $M_S \geq 7.0$ earthquakes from 1977 to 2000 all occurred in the intensive zones of tectonic stresses as observed by satellites.

2. MANTLE CONVECTION GENERATES STRESSES IN THE EARTH

Given a set of fully normalized harmonic coefficients, $C_{n,m}$ and $S_{n,m}$, determined from satellite measurements and surface gravity observations, the relationship between the mantle convection pattern at the upper boundary and the geoid may be described by [2, 3]:

$$\left(\frac{d^2W_n}{dr^2}+\frac{2}{a}\cdot\frac{dW_n}{dr}\right)_{r=a}=\sum_{n=2}^{\infty}\sum_{m=0}^{m=n}\frac{Mg}{4\pi\mu a^2}\left(\frac{a'}{a}\right)^{n+1}\frac{2n+1}{n+1}\overline{P}_n^m(\cos\zeta)\left[\overline{C}_{n,m}\cos(m\lambda)+\overline{S}_{n,m}\sin(m\lambda)\right] \tag{1}$$

where

$M =$ mass of earth, $g =$ gravitational acceleration,

$\mu =$ coefficient of viscosity, $a' =$ radius of the earth,

$a =$ radius of outer spherical surface of the flowing region,

$\overline{P}_n^m(\cos\zeta) =$ associated Legendre polynomial of degree n, order m and argument $\cos\zeta$,

$\lambda =$ the longitude, $\zeta =$ the co – latitude,

$\overline{C}_{2,0}=C_{2,0}-C'_{2,0}$, $\overline{C}_{4,0}=C_{4,0}-C'_{4,0}$,

$\overline{S}_{n,m}=S_{n,m}$, $\overline{C}_{n,m}=C_{n,m}$ for $n \neq 2$ or 4 and $m=0$,

$C'_{2,0}$ and $C'_{4,0} =$ coefficients characterizing the ellipsoid of revolution,

$W =$ a polodal function of convection currents.

In the derivation of equation 1, a Newtonian viscosity is attributed to the mantle and laminar viscous flow is assumed according to Chandrasekhar [28].

If the crust above the flowing mantle is assumed to be an elastic shell, the tangential component of the velocity vanishes at $r = a$, i.e., $\left(dW_n/dr\right)\big|_{r=a}=0$. Then the stress components exerted by the convection flow on the crust in the eastward and northward directions are determined by [10]:

$$\sigma_E(\zeta,\lambda)=-\frac{\mu}{\sin\zeta}\cdot\frac{d}{d\lambda}\left(\frac{d^2W_n}{dr^2}\right)_{r=a}=\sum_{n=2}^{\infty}\sum_{m=0}^{m=n}\frac{Mg}{4\pi a^2}\left(\frac{a'}{a}\right)^{n+1}\frac{2n+1}{n+1}\frac{1}{\sin\zeta}\overline{P}_n^m(\cos\zeta)\left[m\overline{C}_{n,m}\sin(m\lambda)-m\overline{S}_{n,m}\cos(m\lambda)\right] \tag{2}$$

and

$$\sigma_N(\zeta,\lambda)=\mu\frac{d}{d\zeta}\left[\frac{1}{r}\cdot\frac{d}{d\zeta}\cdot\frac{d}{dr}(rW_n)\right]_{r=a}=\mu\frac{d}{d\zeta}\left(\frac{d^2W_n}{dr^2}\right)_{r=a}=\sum_{n=2}^{\infty}\sum_{m=0}^{m=n}\frac{Mg}{4\pi a^2}\left(\frac{a'}{a}\right)^{n+1}\frac{2n+1}{n+1}\cdot\frac{d}{d\zeta}\left[\overline{P}_n^m(\cos\zeta)\right]\cdot$$

$$\left[\overline{C}_{n,m}\cos(m\lambda)+\overline{S}_{n,m}\sin(m\lambda)\right] \tag{3}$$

In order to compute the magnitudes and directions of stresses exerted by the convection currents on the crust, the following recursive relationships among the Legendre and associated Legendre functions were employed [29]:

$$(2n+1)\cos\zeta P_n^0(\cos\zeta)=(n+1)\cos\zeta P_{n+1}^0(\cos\zeta)+nP_{n-1}^0(\cos\zeta) \tag{4}$$

$$P_{n+1}^{m+1}(\cos\zeta)-P_{n-1}^{m+1}(\cos\zeta)=(2n+1)\sin\zeta P_n^m(\cos\zeta) \tag{5}$$

$$(2n+1)\cos\zeta\frac{d}{d\zeta}P_n^0(\cos\zeta)-(2n+1)\sin\zeta P_n^0(\cos\zeta)=(n+1)\frac{d}{d\zeta}P_{n+1}^0(\cos\zeta)+n\frac{d}{d\zeta}P_{n-1}^0(\cos\zeta) \tag{6}$$

$$\frac{d}{d\zeta}P_{n+1}^{m+1}(\cos\zeta)-\frac{d}{d\zeta}P_{n-1}^{m+1}(\cos\zeta)=(2n+1)\sin\zeta\frac{d}{d\zeta}P_n^m(\cos\zeta)+(2n+1)\cos\zeta P_n^m(\cos\zeta) \tag{7}$$

As each function was computed, it was normalized using:

$$\bar{P}_n^m(\mu) = \frac{(2-\delta_{0m})(2n+1)(n-m)!^{1/2}}{(n+m)} P_n^m(\mu) \tag{8}$$

where: $\delta_{0m} = \begin{cases} 0 \text{ if } m \neq 0 \\ 1 \text{ if } m = 0 \end{cases}$

3. STRESS EQUATIONS

The magnitudes and directions of the resultant stresses in the crust associated with mantle convection currents can be expressed by [10]:

$$\sigma(\zeta,\lambda) = \left[\sigma_E^2(\zeta,\lambda) + \sigma_N^2(\zeta,\lambda)\right]^{1/2} \tag{9}$$

and

$$\theta(\zeta,\lambda) = \tan^{-1}\left[\frac{\sigma_N(\zeta,\lambda)}{\sigma_E(\zeta,\lambda)}\right] \tag{10}$$

as shown in Figure 1.

#################################### Figure 1. ####################################

Figure 1. Magnitude and direction of the resultant stress $\sigma(\zeta, \lambda)$ at a grid point (ζ, λ).

Numerical schemes have been programmed for solving equations 2 - 10. Results were obtained at 64,000 grid points having coordinates ζ and λ.

4. SATELLITE GRAVITY DATA: $C_{n,m}$ and $S_{n,m}$

The harmonic coefficients $C_{n,m}$ and $S_{n,m}$ of the geopotential field in equations 2 and 3 have been significantly improved principally because of the improved satellite observations and surface gravity measurements. The harmonics for $n \leq 12$ may reflect a large-scale mantle flow system.

In this paper, we assume the harmonic degree $13 \leq n \leq 25$ and $13 \leq n \leq 150$ to describe the stress field under the crust and in the crust respectively. The Goddard Earth Model-8 (GEM8) for $13 \leq n \leq 25$ is based on the work by Wagner et al. [30].

The input data used in the derivation of this model is made up of 562,000 optical, electronic and laser observations on 27 satellites and 1,656 5° x 5° mean free-air anomalies. Although there remain some statistically questionable aspects of the high-degree harmonics, we have explored their implications for the tectonic forces or stress field under the crust. The development of the joint NASA and National Imagery and Mapping Agency (NIMA) Earth Gravitational Model EGM 96 for $13 \leq n \leq 150$ is based on the work by Lemoine and his 14 co-authors [27]. The input data used in the derivation of the EGM-96 incorporate improved surface gravity data, altimeter-derived gravity anomalies from ERS-1 and from the GEOSAT Geodetic Mission, extensive satellite tracking data including new data from Satellite Laser Ranging (SLR), the Global Positioning System (GPS), NASA's Tracking and Data Relay Satellite System (TDRSS), the French Doris System, and the U.S. Navy TRANET Doppler Tracking System as well as direct altimeter ranges from TOPEX/POSEIDON (T/P), ERS-1, and GEOSAT. The model was used to compute tectonic stresses in the crust.

The recent Catastrophe and Hazard Monitoring and Prediction (CHAMP), Gravity Field Steady State Ocean Circulation (GOCE) and Gravity Recovery and Climate Experiment (GRACE) satellite missions will provide highly accurate measurements of $C_{n,m}$ and $S_{n,m}$ to high degree and order of harmonics [31-33]. We will use the gravity model derived from these satellite missions to refine the tectonic field in the crust of the Earth.

5. STRESSES INFERRED FROM $13 \leq n \leq 25$ DEGREE HARMONICS OF THE GEOPOTENTIAL

The harmonic coefficients $C_{n,m}$ and $S_{n,m}$ in [29] were introduced into equations 2, 3, 9, and 10 to compute the magnitude and direction of the resulting stresses $\sigma(\zeta, \lambda)$. Maps of the subcrustal stresses exerted by mantle convection under Africa, Asia, and Europe taking over one-degree grid and synthesized for $13 \leq n \leq 25$ are shown in Figure 2a, b, c. Divergent arrows indicate tensional stresses in the lithosphere caused by the upwelling mantle flows. Convergent arrows represent compressional stresses in the lithosphere caused by the downwelling mantle flows.

#################################### Figure 2.a b and c ####################################

Figure 2. Subcrustal stresses ($13 \leq n \leq 25$) under: (a) Europe, (b) Asia, and (c) Africa.

It has been shown that the compressional stresses under North China and the tensional stresses under India plate (Figure 2b) caused the 1976 Beijing-Tangshan earthquake in China and the 1993 Latur-Osmanabad earthquake in central India, respectively [14]. Also, we noted that Western Europe is under Northwest-Southeast compressional stresses with the compression centroid located under the Brussels-Liege region in Belgium (Figure 2a). This discovery, from the satellite-derived gravity field, indicated the potential for earthquakes in Europe [34]. Although Western Europe has been seismotectonically stable for centuries, an earthquake did occur in the Liege area on November 8, 1983, just one month after publication of the paper by Liu [24, 25].

6. RECOGNITION AND SIGNIFICANCE OF STRESS PATTERNS

6.1 Stress Pattern Recognition

In principle, three different types of movement in the substratum may cause compression in the overlying crust. These types of movement are illustrated in Figure 3. The first (a) is a decelerating, horizontally directed current, which is transmitted by friction to the overlying crust and courses compression in the direction of flow. Secondly (b), if a descending current forms bilateral or centripetal branches, these will obviously exert compressional force upon the overlying crust. Thirdly (c), uniform but converging current may likewise cause compressional stresses, which in some cases will be parallel to the direction of flow. The compressional stresses in the Tien Shan and Himalayan region in Figure 2b consist of the three flow patterns shown in Figure 3.

#################################### Figure 3. ####################################

Figure 3. Compressional subcrustal stress patterns.

Four different types of movement in the substratum may cause tension in the overlying crust (Figure 4). The first (a) is an accelerating, horizontally directed current, which is transmitted by friction to the overlying crust and causes tension in the direction of flow. Secondly (b), if an ascending current splits into bilateral or centrifugal branches, these will exert tensional force upon the overlying crust. Thirdly (c), horizontal and parallel subcrustal currents of differing velocities will set up torsional forces in the crust, which will give rise to the opening fractures lying obliquely to the direction of flow. Fourthly (d) a uniform but diverging current may cause tensional fractures, which in this case will be parallel to the direction of flow. The tensional stresses in the Tibetan plateau and Baikal rift region in Figure 2b can be explained in terms of stress patterns shown in Figure.4.

################################### Figure 4. ####################################

Figure 4. Tensional subcrustal stress patterns.

6.2 *Significance of Stress Patterns*

In a series of papers, Liu [10, 13-26] has shown that $13 \leq n \leq 25$ stress field has provided an unified forcing mechanism for uplift, depression, rifting, volcanism, seismicity, plate motion, kimberlite magnetism, ore formation, and hot spots distribution on the surface of the Earth. The significance of the subcrustal stresses patterns can be garnered from:

6.2.1 *Seismotectonic Regimes*

The Red Sea and the East African Rift Valley are recognized as major tensional tectonic features of the Earth's crust. The seismicity of the Red Sea, Gulf of Aden, and the East African Rift shows that the Nubian, Arabian, and Somalian plates meet at the south end of the Red Sea (Figure 5a). The relative motions between these three plates have been studied by McKenzie et al. [35]. The results of their calculations are shown in Figure 5a, where the heavy double lines mark the three extensional plate boundaries and the heavy arrows show the relative motion between the plate on which the arrow lies and the adjoining plate. Figure 5a shows that the coincidence in direction of the subcrustal stresses with the relative plate motions in this region can hardly be fortuitous.

Seismic studies, especially fault-plane solutions, can provide further information on the pattern of mantle flows. The stresses derived from fault-plane solutions of earthquakes by Fairhead and Girdler [36] are consistent with the stress field exerted by mantle convection in the region of the East Africa and Red Sea.

Therefore, the relative motions of the tectonic plates and seismic stresses in this region seem to be related to the pattern of the subcrustal stresses. Fault plane solutions of earthquakes show that horizontal tectonic stresses are widespread in central Asia [37-46]. The principal axes of compressional and tensional stresses from fault plane solutions of earthquakes in this region are plotted in Figure 5b.

From fault plane solutions of earthquakes, a north-south compression system in the Himalayan frontal thrust has been established. Much of the late Cenozoic history of the Tibetan plateau is characterized by east-west tension, however, in the Tien Shan and south Mongolian region there is again north-south compression. North of Mongolia, compressive stress gives way to tensional stress, causing normal faulting in the Baikal rift system. The convection-generated stresses or forces in Figure 5b explain all these fault-plane solutions clearly and simply. In all regions in Figure 5b, regardless of structure and all other characteristics, systematic horizontal compression and tension is observed. The system of compressive or tensional zones and the persistence of their topographic characteristics are consistent with only one zoning mechanism, namely the upwelling and downwelling of mantle material. In these regions, there exists a clear-cut correlation between the convection-generated stresses and the directions of the principal stresses derived from fault plane solutions of earthquakes. The convection-generated stress concentration should occur in narrow fault zones and causes earthquakes [14].

The subcrustal stresses under the Baikal-Stanovoy region of Eastern Siberia [23] are shown in Figure 5c, which illustrates several consistent stress patterns including the remarkable tensional stress field under the Baikal rift zone and the north-south compression in the Stanovoy Range region. These stress patterns in Figure 5c are in good agreement with stress orientation of earthquake foci along the Baikal-Stanovoy seismic belt as shown in Figure 5d by Misharina [47-50]. Particularly, they have provided a geodynamical explanation for the puzzling seismic gap along the Baikal-Stanovoy seismic belt in Figure 5d.

################################### Figure 5 a b c and d . ##################################

Figure 5. (a) The directions of subcrustal stresses are in good agreement with the relative plate nations in the East Africa and Red Sea region. (b) The principal axes of compressional and tensional stresses from fault plane

solutions of earthquakes in Central Asia are in good agreement with the subcrustal stresses. (c) Subcrustal stresses under the Baikal-Stanovoy region of Eastern Siberia. (d) Stress orientation of earthquake foci along the Baikal-Stanovoy seismic belt.

6.2.2 Volcanism and Hot Spots

Hot spots on the Earth's surface, marked by anomalous volcanism, could be surface expressions or flaws of stress concentration in tension caused by the hotter upwelling mantle convection currents. Widespread Cenozoic intra-plate volcanism in Africa, Australia, and the Western United States as shown in Figure 6a, b, c, and d is almost exclusively restricted to areas of the convection generated tensional stress field. This non-random distribution indicates that during Cenozoic the convection generated stresses in the lithosphere have exerted a control on the locations of these volcanic areas. In this case, intra-plate volcanism would be associated with tensional tectonics. The absence of volcanism in the convection generated compressional stress regimes implies that the environment of compression in the lithosphere is unfavorable for basalt magmas to migrate from the asthenosphere to the surface of the Earth [18].

Mantle plume hypothesis is one of the possible explanations for intra-plate volcanism [51, 52]. Ascending convection can lead to pressure-release melting and the magmas penetrate the lithospheric plate in tension leading to volcanism. Areas of anomalous volcanism are often referred to as hot spots. The global distribution of 122 hot spots has been shown by Wilson [51] and Burke and Wilson [52]. Hot spots are not uniformly distributed over the surface of the Earth. There are numerous hot spots in Africa as shown in Figure 6d, none in South America, and relatively few in North America, Eurasia and Australia.

Close examination of the global distribution of hot spots in relation to the convection generated stress field shows that 122 hot spots are restricted to the tensional stress regimes exerted by the upwelling mantle convection currents. This restricted distribution of hot spots on the surface of the Earth indicates that the mantle convection flows as inferred from the satellite and surface gravity data have exerted a control on the locations of the hot spots. Therefore, hot spots on the surface of the Earth, marked by volcanism, high heat flow and uplift, may be the surface expressions or flaws of stress concentration in tension caused by the hotter upwelling mantle convection cells.

#################################### Figure 6 a b c and d . #####################################

Figure 6. Volcanism and hot spots. Cenozoic intra-plate volcanism in (a) Africa, (b) Australia, and (c) Western United States could be surface expression of subcrustal stress concentration in tension. (d) 32 hot spots in Africa are restricted to the tensional subcrustal stress regimes.

6.2.3 Metal Deposits

African magmatism is largely related to the tensional stress regimes of the crust which are induced by the hotter upwelling mantle rocks. These mantle rocks may provide emanating forces and thermal energy for the upward movements of primary ore bodies with fluid inclusions in the tensional stress regimes of the crust. The subcrustal stress system exerted by mantle convection under Africa is found to be correlated with the African metallogenic provinces [22]. Recognition of the full spectrum of ore deposits in Africa that may be associated with the hotter upwelling mantle rocks has provided independent evidence to support the hypothesis of mantle-derived heat source for ore deposits.

The output of metals from Africa is prodigious in quantity and value and manifold in character. The specific and more localized provinces of metal concentrations in Africa were published in the Mineral Map of Africa by UNISCO. The distribution of the 450 principal deposits of antimony, bauxite, beryl, chrome, cobalt, copper, gold, tin, iron, manganese, niobium, tantalum, platinum, pyrite, uranium, vanadium, zinc, and lead in relation to the stress systems in the lower crust due to mantle convection are shown in Figure 7. Figure 7 shows that all ore deposits are clustered in areas of uplifted old rocks. These findings seem to suggest that ore deposits of all ages in Africa were exposed by stress induced uplift.

Under the central area of Africa, the colder downwelling mantle flows are compatible with the crustal condition of a group of basins. Since the lithosphere of central Africa is under compression due to the colder downwelling mantle flows, ore deposits associated with fluid inclusions under crustal compression without heat source may be still confined in the basement rocks. We have no way of knowing what ore deposits distribution pattern may be in this area. However, the unsuccessful and intensive geological explorations in the compressional stress field of North China have answered the doubts in a positive sense that such information may be useful for the exploration geoscientists [14].

The difficulty that many geologists have had in accepting the formation of ore deposits from water-rich fluids of magmatic origin has not been so much the physical characteristics of the ores themselves as the problems of how they were transported to the surface of the Earth. Many of those geologists who still believe that the physical relationships of primary ore bodies to the rocks which enclose them indicate an upward direction of ore-fluid movement will find support for their position in the application of stress distribution calculated from the satellite determined gravity anomalies.

#################################### Figure 7. #####################################

Figure 7. The 450 principal ore deposits in Africa are clustered and exposed by the tensional subcrustal stress field.

7. STRESSES INFERRED FROM $13 \leq n \leq 150$ DEGREE HARMONICS OF THE GEOPOTENTIAL

The harmonic coefficients $C_{n,m}$ and $S_{n,m}$ in [27] were introduced in to equations 2, 3, 9, and 10 to compute the magnitude and direction of the stresses in the crust exerted by mantle convection, taking one-degree grid and synthesized for $13 \leq n \leq 150$. The global crustal stress patterns are shown in Figure 8. The length of the arrows represents the magnitude of the stress strength. Figure 8 seems to suggest a stress origin of shaping our world. Large earthquakes may be restricted in the global stress belts and stress concentration zones.

#################################### Figure 8. #####################################

Figure 8. Global tectonic stress map for $13 \leq n \leq 150$.

Large earthquakes ($M_S \geq 7.0$) data from USGS earthquake hazard program are listed in Table 1 for 1977 - 2000.

#################################### Table 1. #####################################

We have plotted the locations of these listed large earthquakes ($MS \geq 7.0$) on Figure 9.

#################################### Figure 9. #####################################

Figure 9. Distribution of large earthquakes ($M_S \geq 7.0$) from 1977 to 2000 over the world.

Examination of Figures 8 and 9 shows that the 131 $MS \geq 7.0$ earthquakes are indeed restricted in the stress belts and stress concentration zones. It is highly probable that the satellite detected stresses in Figure 8 are the triggering stresses [53] for large earthquakes.

8. FORMATION OF SEISMOTECTONIC BELTS

Satellite detected stress belts are particularly intense in the ring of fire around the Pacific as indicated by strong convergence of arrows in Figure 10. These are the Western U. S. , the Andes and the associated ocean trench, off the Tonga trench, the Japan trench, and near the East Indies. An important aspect of these stress belts relative to earthquakes is the implication for seismic hazard assessment. Kossobokov et al. [53] and Turcotte et al. [54] proposed a systematic global assessment of the seismic hazard based on the extrapolation of the occurrence of earthquakes. They developed a statistical physics approach to earthquakes for probabilistic seismic hazard on extrapolations of available data. Their method was based on the epicenters of earthquakes taken from the Global Hypocenter Database of the U. S. National Earthquake Information Center. The statistically significant advance prediction is shown in Figure 11 [53]. It should be noted that the World Stress Map Project [55] has compiled seismic stress data and the earthquake data were used for studies of triggered earthquakes [56].

#################################### Figure 10. #####################################

Figure 10. Satellite detected stress belts in the ring of fire around the Pacific.

##################################### Figure 11. #####################################

Figure 11. Statistically significant advance prediction of the Circum-Pacific seismic belts.

Examination of Figures 10 and 11 shows that the satellite observed stress belts in Figure 10 and the statistically predicted seismic belts in Figure 11 [53] are closely correlated. It seems reasonable to suggest that the triggering stresses of the earthquakes in the ring of fire around the Pacific can be detected by satellites.

9. CONCLUSION

Satellite detection of convection-generated stresses in the interior of the Earth has a history in space and Earth sciences. It has been one of the most impressive and important Earth research program since the beginning of the space age. This program is applicable for identification of the forcing mechanisms for uplift, depression, rifting, volcanism, seismicity, plate motion, kimberlite magmatism, ore formation, and hot spots distribution on the surface of the Earth. It is shown that distribution of the 450 principal metal deposits in Africa is restricted in the tensional stress system and all ore deposits are clustered in areas of the uplifted old rocks, indicating that metal deposits of all ages in Africa were exposed by stress induced uplift. Most importantly, we have demonstrated that the intensive compressional and tensional stresses in the global stress concentration belts are the triggering stresses for the 131 $M_s \geq 7.0$ earthquakes for 1977 to 2000. Therefore, we conclude that recent research development in this special field of geophysics has provided a direct approach to seismic hazard assessment and Earth resources survey.

ACKNOWLEDGEMENT

This paper is dedicated to the memory of S. Chandrasekhar, J. A. O'Keefe and S. K. Runcorn who saw that it must be true. We thank F. G. Lemoine and his research team members for providing satellite gravity data for our research development.

REFERENCES

1. O'Keefe, J. A., 1959, J. Geophys. Res., 64, 2389.
2. Runcorn, S. K., 1964, J. Geophys. Res., 69, 4389.
3. Runcorn, S. K., 1967, J. R. Astron. Soc., 14, 375.
4. Richter, F. M. and Parson, B., 1975, J. Geophys. Res., 80, 2529.
5. Marsh, B. D. and Marsh, J. G., 1975, EOS (Am. Geophys. Union) 56, 1063 (abstract).
6. Turcotte, D. L. and Oxburgh, E. R, 1973, Nature, 244, 337.
7. McKenzie, D. P., Roberts, J. M., and Weiss, N. O., 1974, J. Fluid Mech., 62, 465.

8. G. Schubert, D. L. Turcotte, and P. Olson, 2001, Mantle Convection in the Earth and Planets, Cambridge U. Press, 956 pp.
9. Liu, H. S., 1974, J. Geophys. Res., 79, 2568.
10. Liu, H. S., 1976, Phys. Earth Planet Inter., 13, 212.
11. Jeffreys, H., 1962, The Earth, 4th ed., Cambridge U. Press, 328 pp.
12. Hide, R. and Horai, K., 1968, Earth Planet Inter., 1, 305.
13. Liu, H. S., 1977, Phys. Earth Planet Inter., 15, 60.
14. Liu, H. S., 1978, Phys. Earth Planet Inter., 16, 247.
15. Liu, H. S., 1979, Phys. Earth Planet Inter., 19, 307.
16. Liu, H. S., 1979, Modern Geology, 7, 29.
17. Liu, H. S., 1979, Bull. of Seismological Soc. of Am., 69, 1989.
18. Liu, H. S., 1980, Tectonophysics, 65, 225.
19. Liu, H. S., 1980, Modern Geology, 7, 81.
20. Liu, H. S., 1980, Modern Geology, 7, 161.
21. Liu, H. S., 1981, Phys. Earth Planet Inter., 25, 64.
22. Liu, H. S., 1981, Modern Geology, 8, 23.
23. Liu, H. S., 1982, Phys. Earth Planet Inter., 31, 77.
24. Liu, H. S., 1983, Phys. Earth Planet Inter., 32, 146.
25. Liu, H. S., 1984, in Seismic Activity in Western Europe, ed. by Melchior, P., Reidel, 448 pp.
26. Liu, H. S., 1985, Phys. Earth Planet Inter., 40, 43.
27. Lemoine, F. G. and 14 co-authors, 1998, NASA/TP-1998-206861.
28. Chandrasekhar, S., 1961, Hydrodynamic and Hydromagnetic Stability, Oxford U. Press.
29. Arfken, G., 1966, Mathematical Methods for Physicists, Academic Press, New York, N. Y., 423.
30. Wagner, C. A., Lerch, F. J., Brown, J. E., and Richardson, J. A., 1977, J. Geophys. Res., 82, 901.
31. Reigber, C., 2001, EOS Trans AGU, 82 (47), F286.
32. Suenkel, H., 2001, EOS Trans AGU, 82 (47), F286.
33. Tapley, B. D., 2001, EOS Trans AGU, 82 (47), F286.
34. Melchior, P., 1984, Seismic Activity in Western Europe, Reidel, 448 pp.
35. McKenzie, D. P., Davis, D., and Molnar, P., 1970, Nature, 226, 1-6.
36. Fairhead, J. D. and Girdler, R. W., 1971, Geophys. J. R. Astron. Soc., 24, 271.
37. Ritsema, A. R., 1961, Geophys. J. R. Astron. Soc., 5, 254.
38. Molnar, P. and Tapponnier, P.,1975, Science 189, 419.
39. Molnar, P., Fitch, T. J., and Wu, F. T., 1973, Earth Planet Sci. Lett., 19, 101.
40. Molnar, P. and Tapponnier, P.,1978, J. Geophys. Res., 83, 5361.
41. Ni, J., 1978, Earth Planet Sci. Lett., 41, 347.
42. Ni, J. and York, J. E., 1978, J. Geophys. Res., 83, 5377.
43. Rastogi, B. K., 1976, Bull. Inst. Seismol. Eng., 14, 99.
44. Riznichenko, Y. V., 1972, Phys. Earth Planet Inter., 6, 211.
45. Shirokova, E. I., 1974, Izv. Acad. Sci. USSR, Phys. Solid Earth, 11, 22.
46. Yeh, H., Liang, Y. S., Shen, L. R., and Xiang, H. F., 1975, Sci. Geol. Sin., 1, 32.
47. Misharina, L. A., 1972, In: N. V. Solonenko (Editor), The Field of Elastic Stresses and Earthquake Mechanisms. Seismology, 8: 161.
48. Misharina, L. A. and Solonenko, N. V., 1977, In: N. A. Logachev (Editor), The Role of Rifting in the Earth's Geological History. Nauka, Novosibirsk, 120.
49. Misharina, L. A., Solonenko, N. V., and Leonteva, L. R., 1975, In: N. A. Florensov (Editor), The Baikal Rift. Nauka, Novosibirsk, 9.
50. Misharina, L. A., Solonenko, N. V., and Vertlib, M. B., 1977, In: N. V. Solonenko (Editor), Seismicity of Eastern Siberia, Nauka, Moscow, 43.
51. Wilson, J. T., 1973, Tectonophysics, 19, 149.
52. Burke, K. and Wilson, J. T., 1972, Nature, 239, 387.
53. Kossobokov, V. G., Romashkova, L. L., Keilis-Borok, V. I., and Healy, J. H., 1999, Phys. Earth Planet Inter., 111, 187.

54. Turcotte, D. L., Newman, W. J., and Gabrielov, A., 2000, Geophys. Monograph 120, 83.
55. Zoback, M. L., 1992, J. Geophys. Res., 97, B8, 11703.
56. Parsons, T., 2002, J. Geophys. Res., 107, B9, 2199.

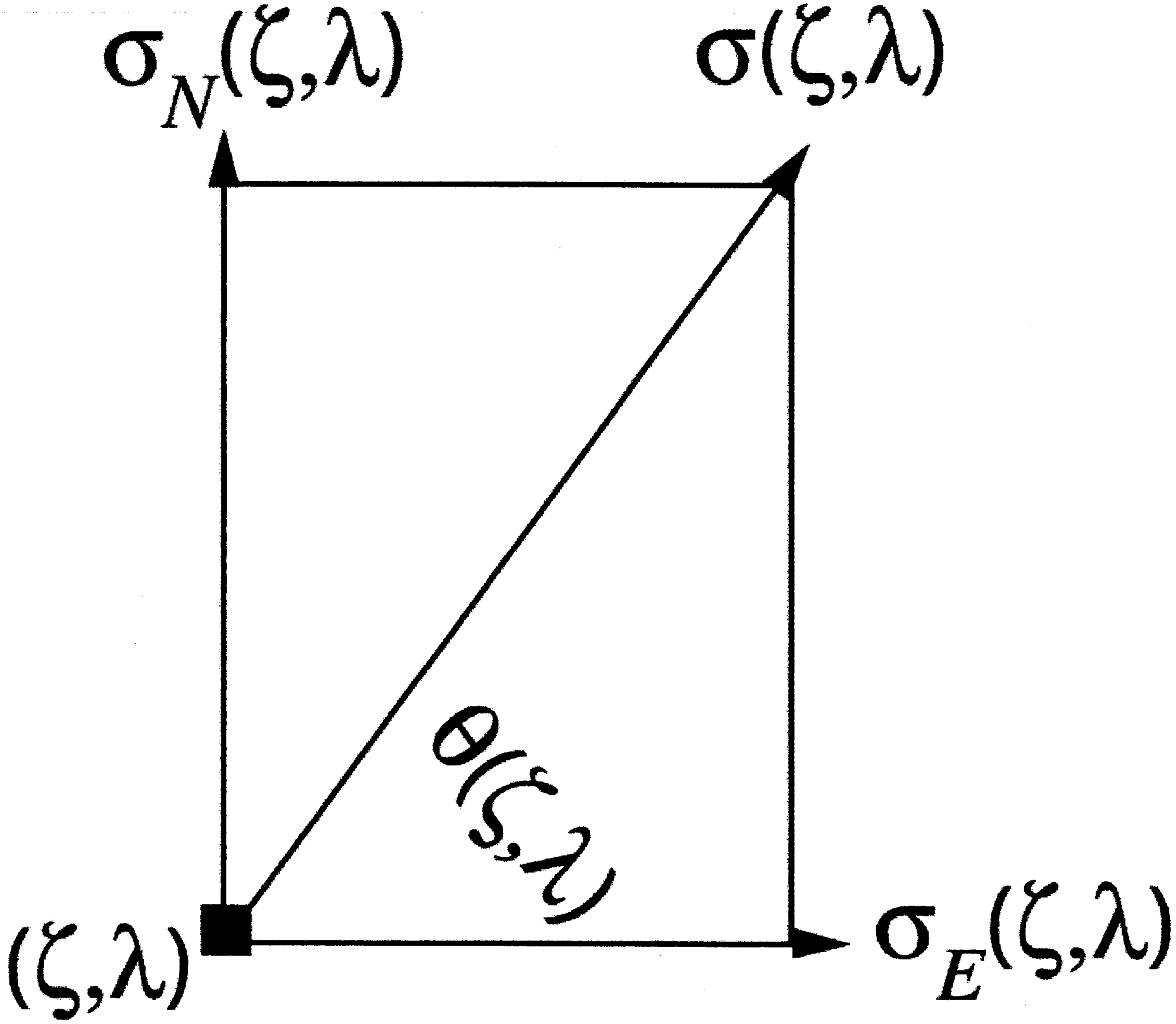

Figure 1. Magnitude and direction of the resultant stress $\sigma(\zeta, \lambda)$ at a grid point (ζ, λ).

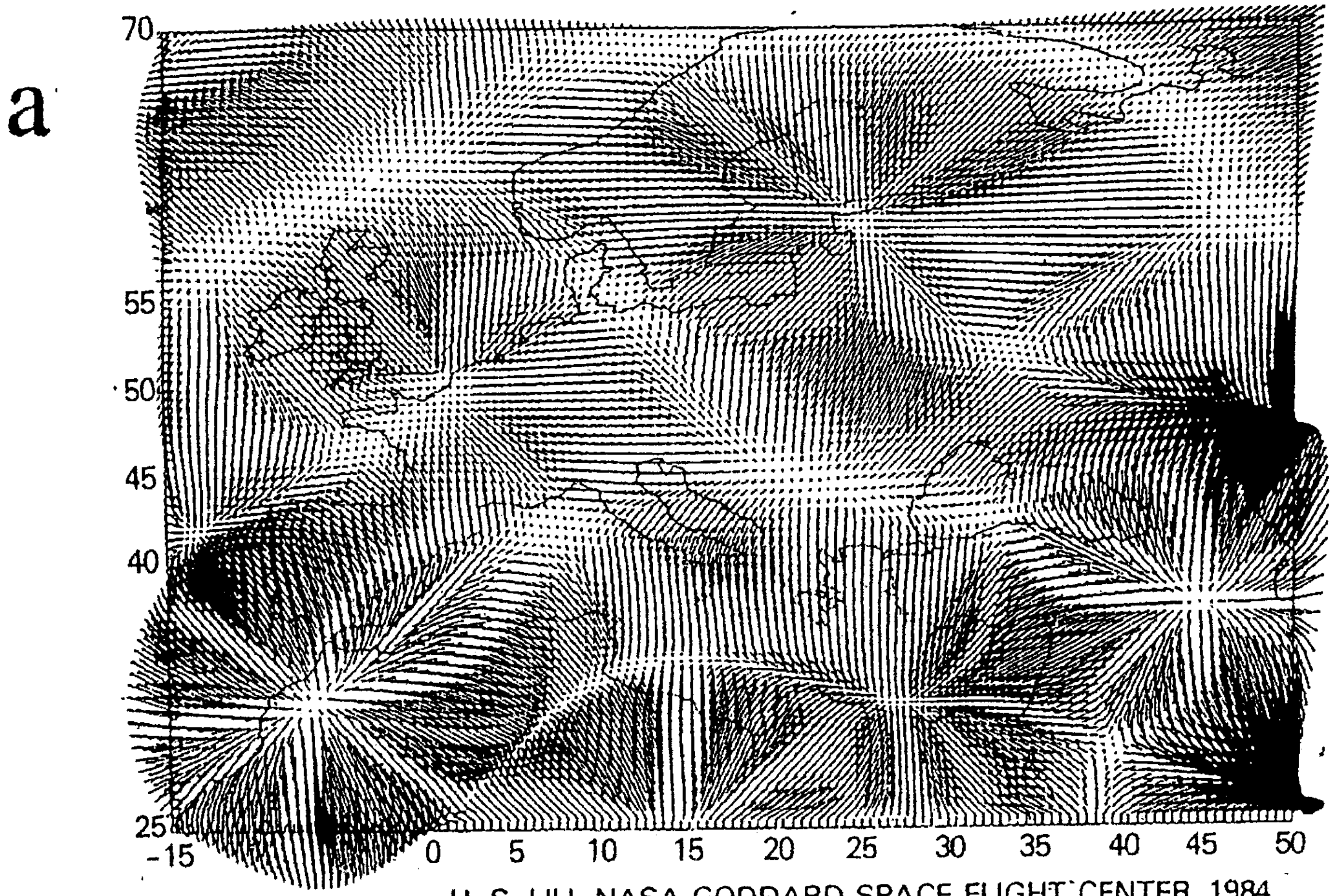

H. S. LIU, NASA GODDARD SPACE FLIGHT CENTER, 1984.

Figure 2. (a) Europe

b

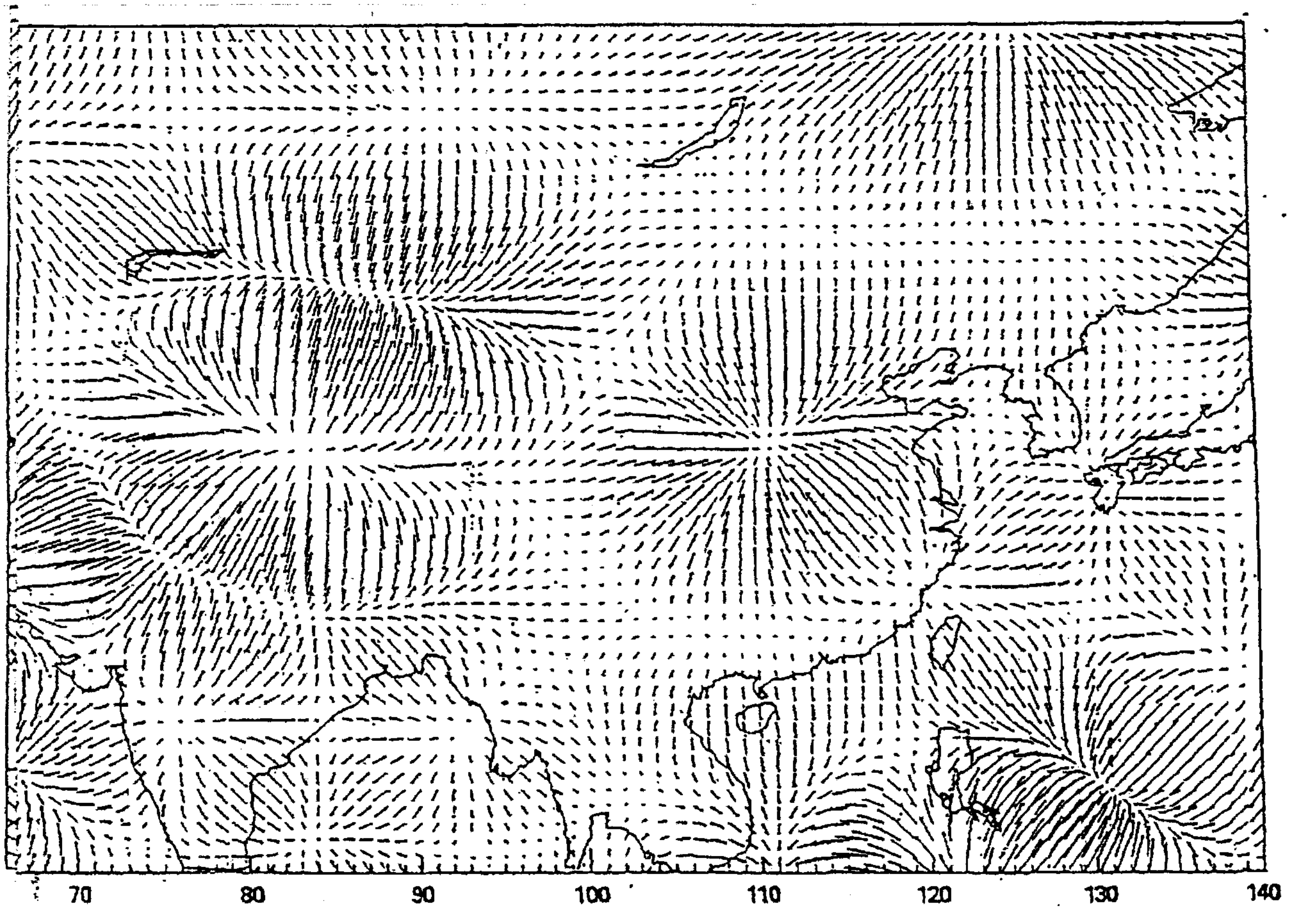

Figure 2. (b) Asia

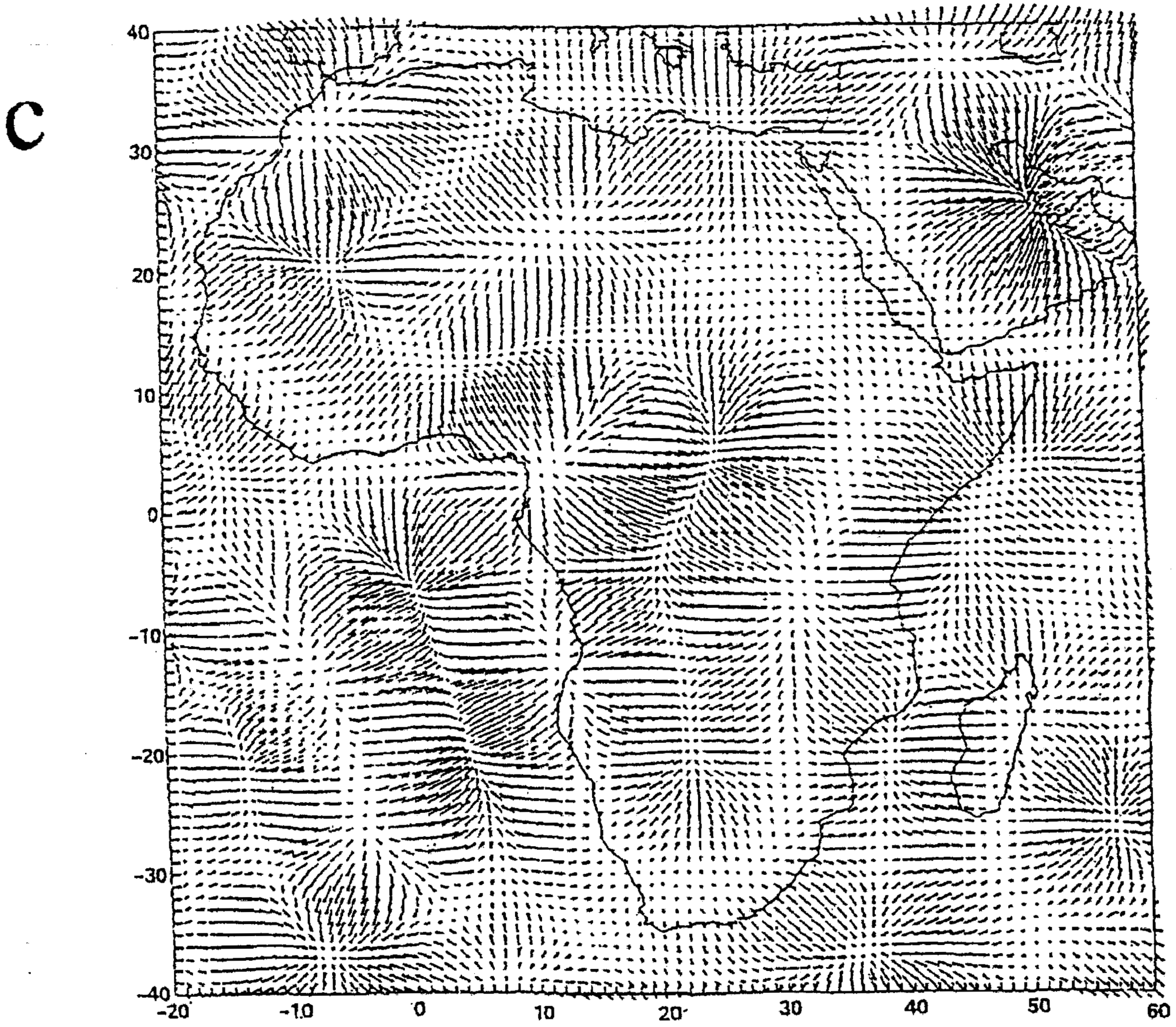

Figure 2. (c) Africa.

Figure 2. Subcrustal stresses ($13 \leq n \leq 25$) under: (a) Europe, (b) Asia, and (c) Africa.

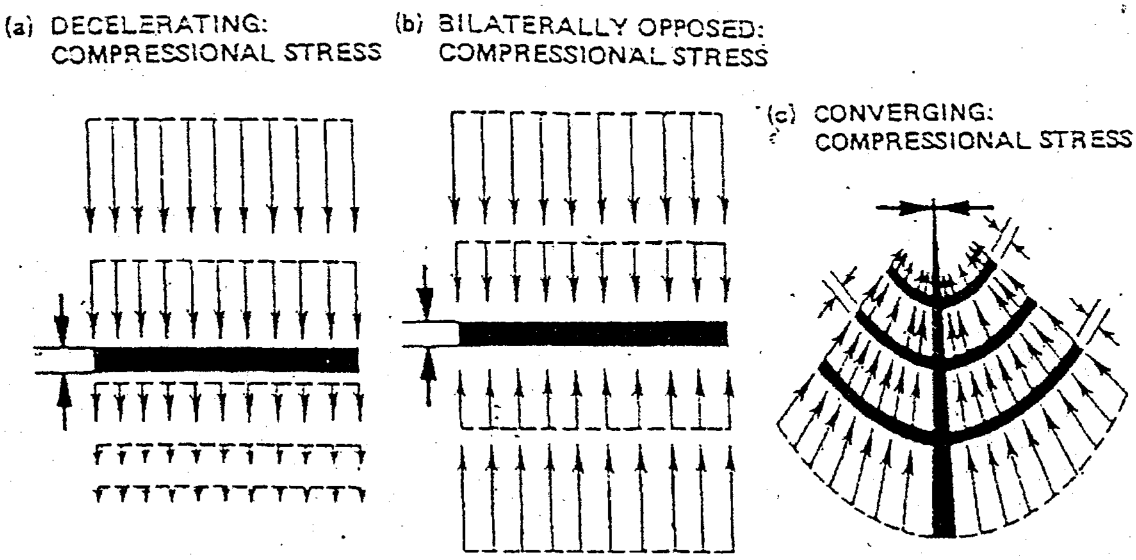

Figure 3. Compressional subcrustal stress patterns.

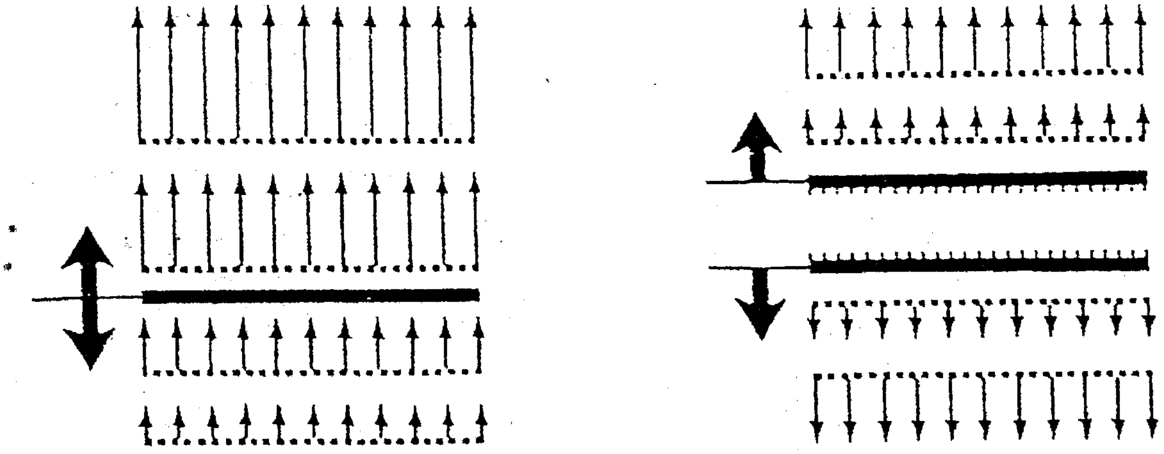

(a) Accelerating: tensional fissures ⊥

(b) Bilaterally opposed: tensional graben

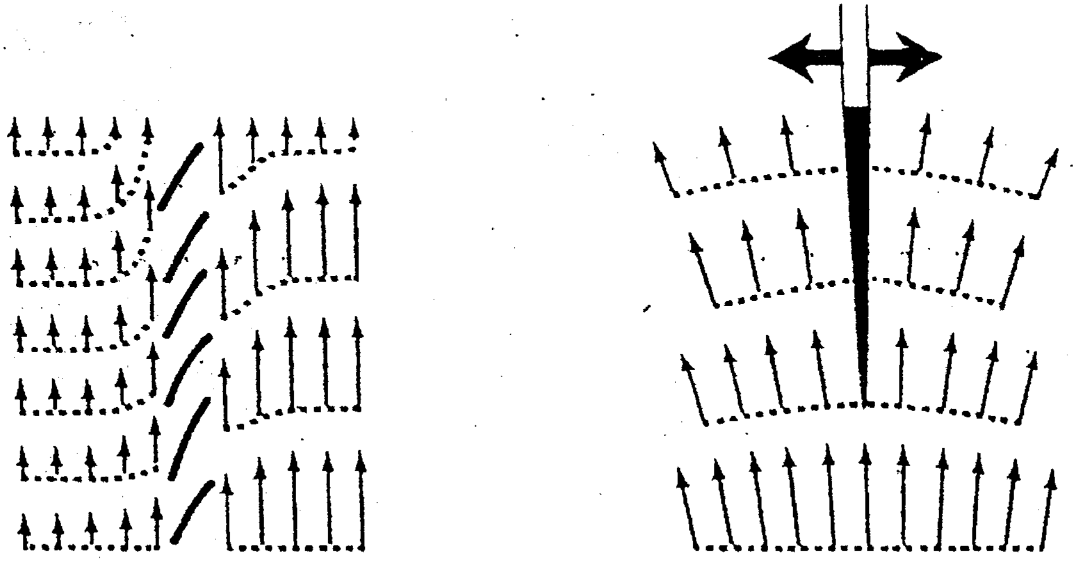

(c) Unequal parallel: feather fissures

(d) Diverging: tensional fissures ||

Figure 4. Tensional subcrustal stress patterns.

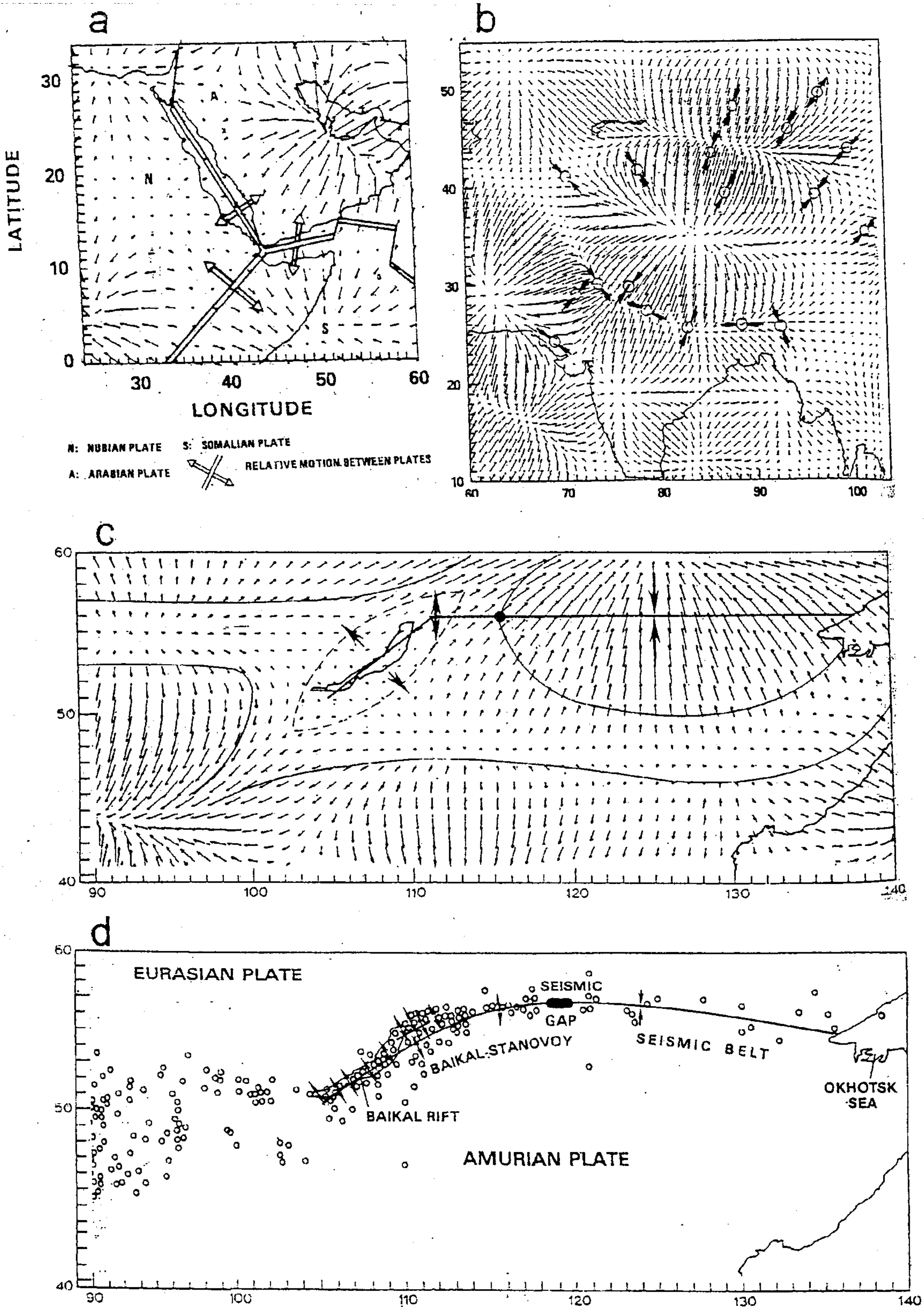

Figure 5. (a) The directions of subcrustal stresses are in good agreement with the relative plate nations in the East Africa and Red Sea region. (b) The principal axes of compressional and tensional stresses from fault plane solutions of earthquakes in Central Asia are in good agreement with the subcrustal stresses. (c) Subcrustal stresses under the Baikal-Stanovoy region of Eastern Siberia. (d) Stress orientation of earthquake foci along the Baikal-Stanovoy seismic belt.

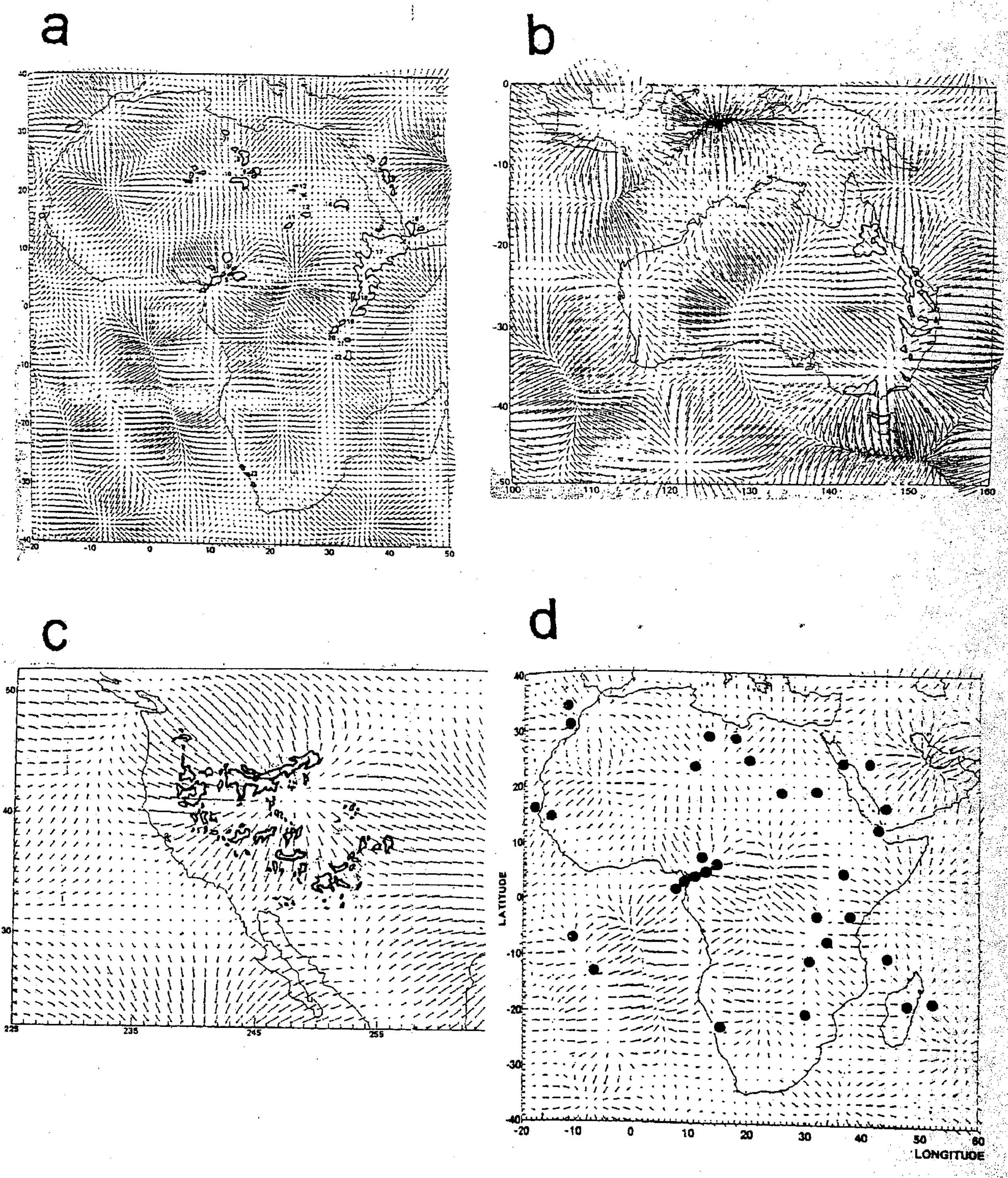

Figure 6. Volcanism and hot spots. Cenozoic intra-plate volcanism in (a) Africa, (b) Australia, and (c) Western United States could be surface expression of subcrustal stress concentration in tension. (d) 32 hot spots in Africa are restricted to the tensional subcrustal stress regimes.

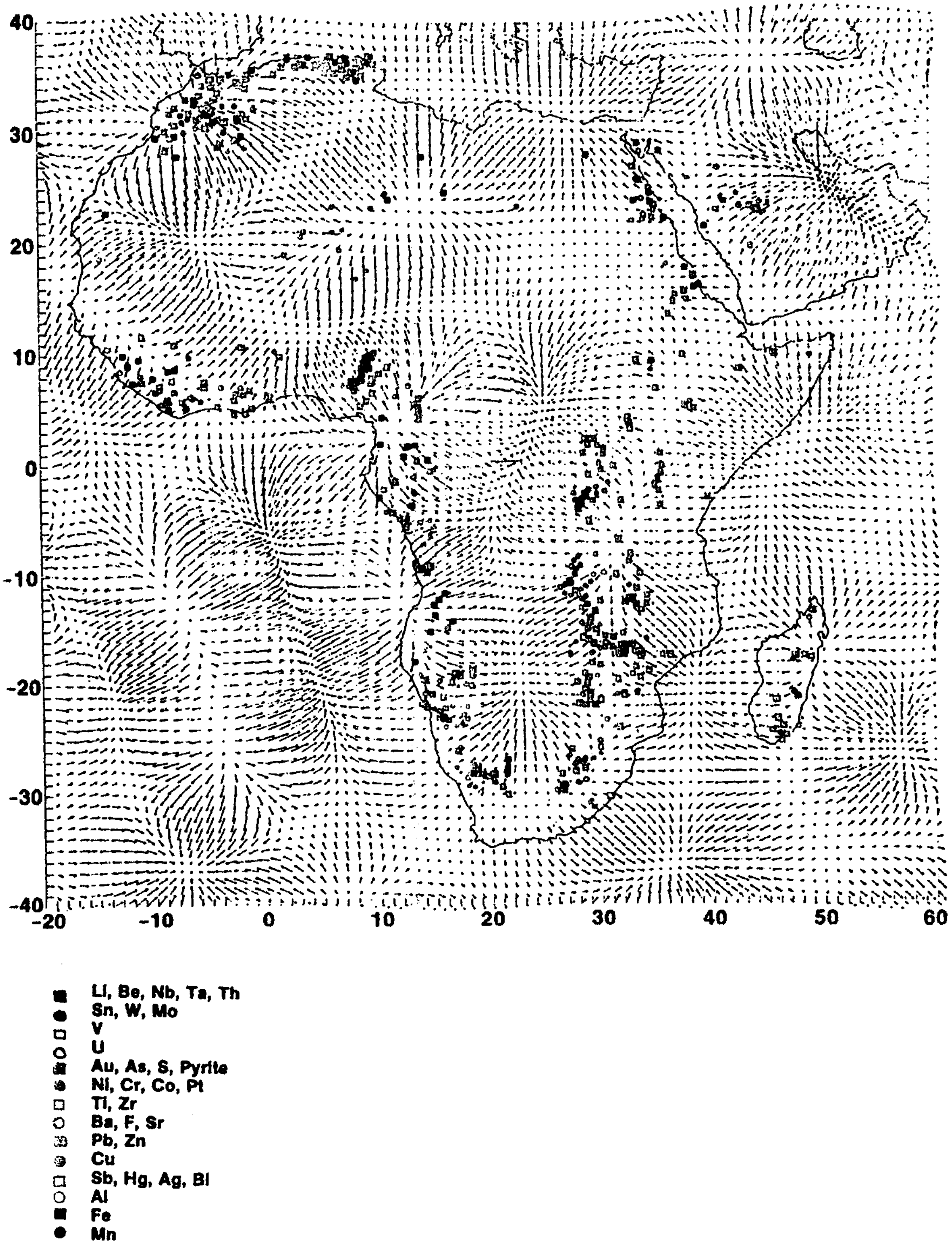

Figure 7. The 450 principal ore deposits in Africa are clustered and exposed by the tensional subcrustal stress field.

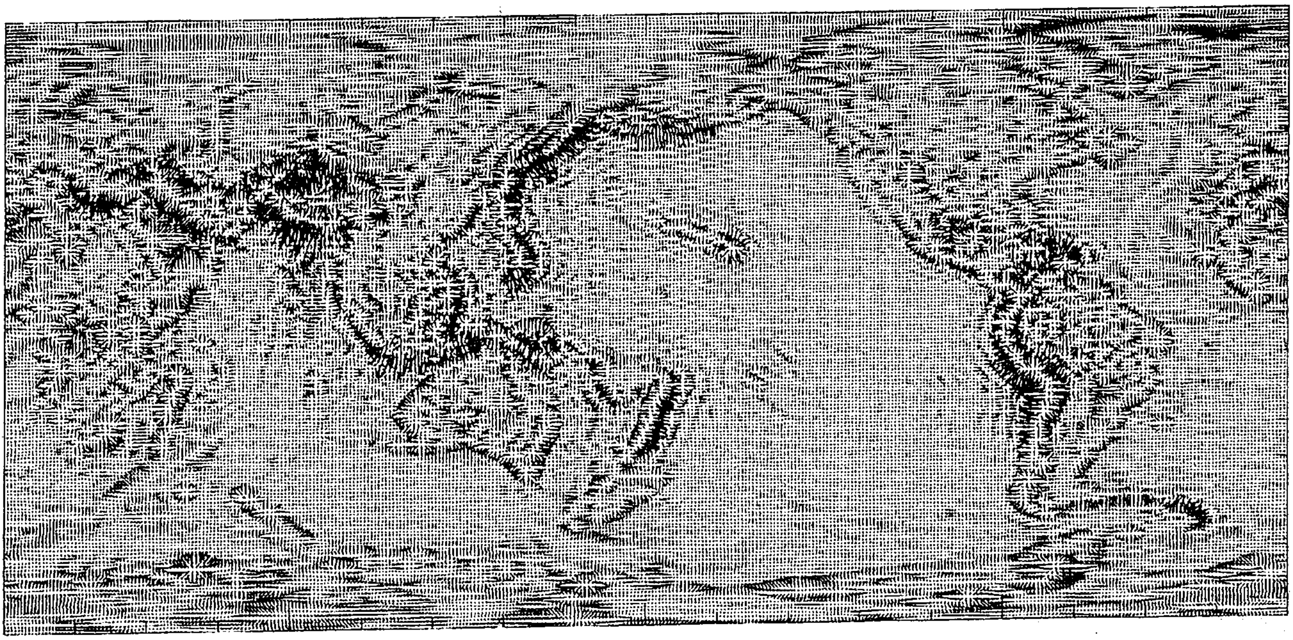

Figure 8. Global tectonic stress map for $13 \leq n \leq 150$.

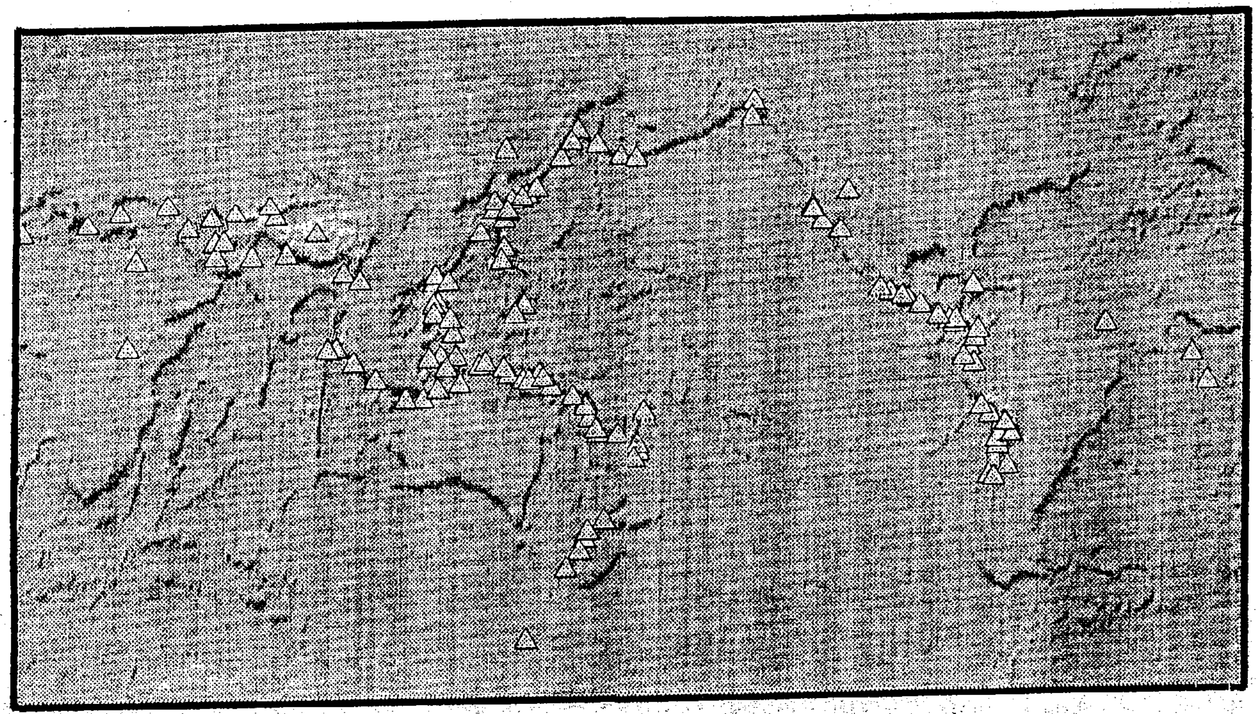

Figure 9. Distribution of large earthquakes ($M_S \geq 7.0$) from 1977 to 2000 over the world.

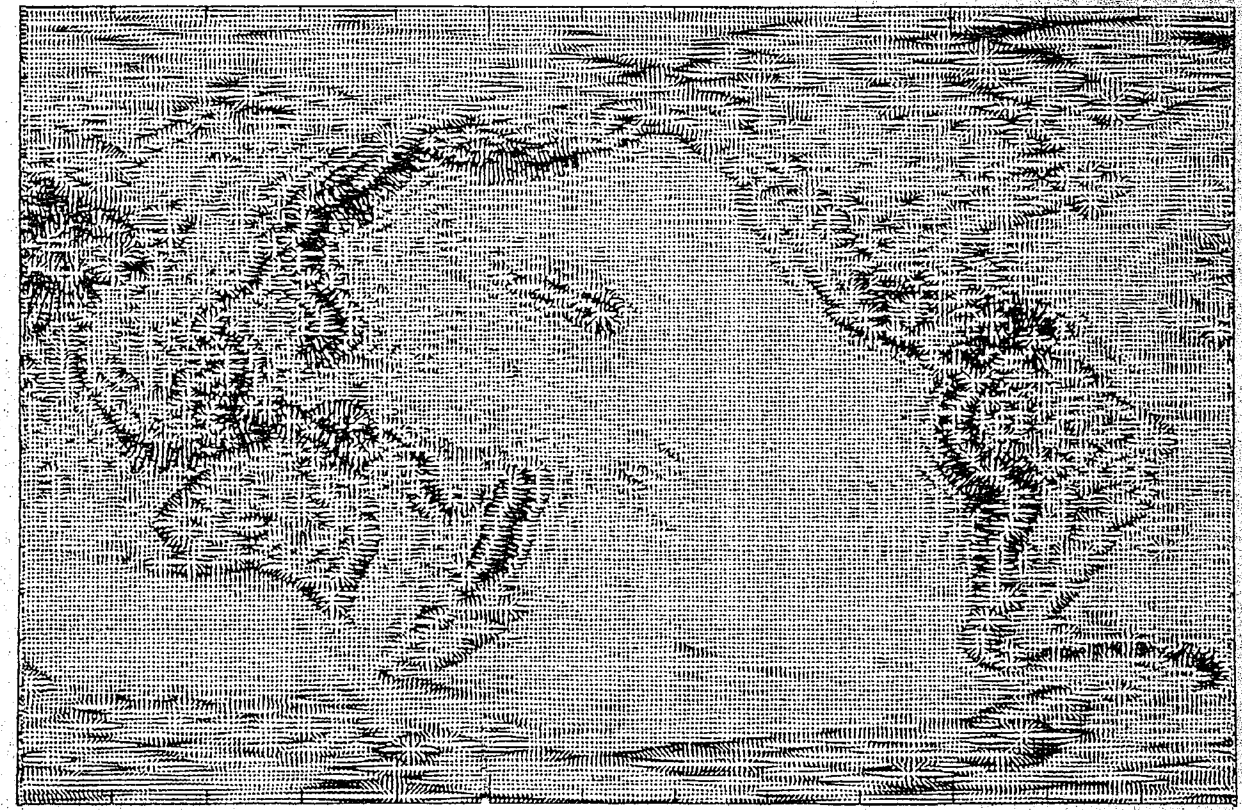

Figure 10. Satellite detected stress belts in the ring of fire around the Pacific.

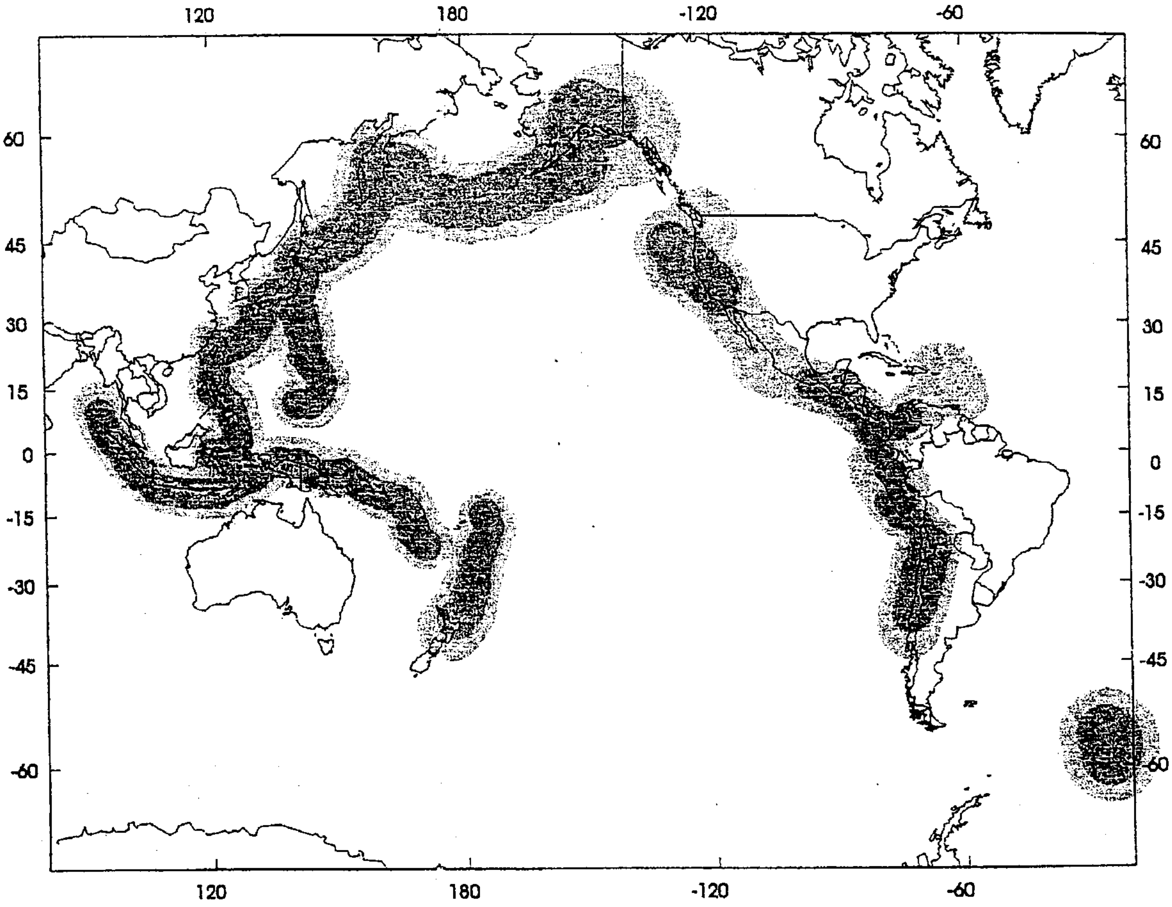

Figure 11. Statistically significant advance prediction of the Circum-Pacific seismic belts.

Table 1.The 131 $M_S \geq 7.0$ Earthquakes used in this study.

Earthquake	Date	M_S	Latitude	Longitude
Luzone	1977	7.0	16.3	122.5
Solomon Islands	1977	7.2	-8.1	155.9
Sumba	1977	7.9	-11.1	118.3
Tonga Islands	1977	7.4	-26.1	-174.8
Argentina	1977	7.4	-31.2	-67.6
Kermadec Islands	1978	7.2	-30.6	-177.0
Kuril Islands	1978	7.5	44.1	149.2
Japan	1978	7.7	38.0	142.0
Taiwan Region	1978	7.4	22.0	121.6
Iran	1978	7.4	33.3	57.4
Mexico	1978	7.7	16.2	-96.5
Alaska	1979	7.3	60.5	-141.3
Mexico	1979	7.6	17.7	-101.3
Irian Java	1979	7.9	-1.7	136.0
New Zealand	1979	7.4	-46.5	165.7
Colombia	1979	7.7	2.3	-78.8
Kuril Islands	1980	7.0	43.2	146.9
Santa Cruz Islands	1980	7.5	-12.9	166.2
Algeria	1980	7.3	36.2	1.3
Loyalty Islands	1980	7.2	-21.7	169.8
Eureka, California	1980	7.2	41.1	-124.3
Rat Islands	1981	7.0	51.5	176.1
New Zealand	1981	7.6	-48.9	164.3
Vanuatu Islands	1981	7.1	-17.3	167.2
Iran	1981	7.1	30.0	57.5
Samoa Islands	1981	7.7	-15.0	-173.1
Michoacan	1981	7.3	18.2	-102.0
Mexico	1982	7.0	16.9	-98.3
Greece	1983	7.0	38.1	20.3
Costa Rica	1983	7.2	8.8	-83.2
Japan	1983	7.7	40.4	138.8
Chile	1983	7.3	-26.0	-70.5
Idaho	1983	7.3	44.3	-113.9
Uzbekistan	1984	7.0	40.5	63.2
Kuril Islands	1984	7.1	44.1	148.6
Mid-Atlantic Ridge	1984	7.1	8.3	-38.8
North Sumatera	1984	7.2	-0.2	97.8
Kamchatka	1984	7.0	56.2	163.8
Chile	1985	7.8	-33.9	-71.7
New Britain	1985	7.1	-5.6	150.9
New Britain	1985	7.2	-4.2	152.5
West Irian	1985	7.1	-1.6	134.7
Vanuatu	1985	7.0	-14.0	166.0
Andreanof Islands	1986	7.7	51.3	-175.4
New Guinea	1986	7.1	-4.4	143.6
Kermadec Islands	1986	8.2	-27.9	-176.0
Taiwan	1986	7.8	23.9	121.8

New Guinea	1987	7.4	-5.9	147.7
Chile	1987	7.3	-24.3	-70.9
New Britain	1987	7.4	-6.2	149.4
Alaska	1987	7.6	58.1	-142.0
Peru	1988	7.0	-17.5	-72.8
Burma	1988	7.2	25.1	94.8
China	1988	7.3	23.0	99.6
Macquarie Ridge	1989	8.3	-52.1	160.4
Loma Prieta	1989	7.1	37.0	-121.6
Solomon Islands	1989	7.1	-10.9	162.3
Japan	1989	7.3	39.9	143.0
Philippines	1989	7.4	7.8	126.9
Fiji	1990	7.5	-22.0	175.3
Costa Rica	1990	7.0	9.9	-84.5
Mariana Islands	1990	7.5	15.5	148.0
Minanasa Peninsula	1990	7.4	1.3	123.3
Sudan	1990	7.2	5.3	32.2
Iran	1990	7.7	36.9	49.5
Philippines	1990	7.7	15.9	121.2
Komandorsky Is.	1990	7.0	53.7	169.4
Costa Rica	1991	7.5	10.1	-82.7
Caucasus	1991	7.0	42.6	43.6
Northern India	1991	7.1	30.2	78.2
Columbia	1991	7.0	4.8	-77.1
Kuril Islands	1991	7.4	45.5	151.5
Cape Mendocino	1992	7.1	40.2	-124.3
Landers	1992	7.5	34.6	-116.6
Kyrgyzstan	1992	7.4	42.1	73.3
Ascension Island	1992	7.0	-0.7	-13.5
Nicaragua	1992	7.2	11.2	-87.8
Colombia	1992	7.3	7.2	-76.3
Indonesia	1992	7.5	-8.3	122.4
Hokkaido	1993	7.1	43.0	144.2
Kamchatka	1993	7.3	51.3	158.7
Guam	1993	8.1	13.0	145.3
New Zealand	1993	7.1	-45.0	166.7
Guatemala	1993	7.3	14.4	-92.9
Indonesia	1994	7.2	1.2	127.8
Vanuatu Islands	1994	7.2	-20.4	169.0
Indonesia	1994	7.0	-5.1	104.2
Java	1994	7.2	-11.0	113.0
New Zealand	1994	7.1	-42.9	171.4
Kuril Islands	1994	8.1	43.7	147.3
Philippines	1994	7.1	13.4	121.3
Japan	1994	7.5	40.5	142.9
Tonga	1995	8.0	-15.3	-173.1
Philippines	1995	7.0	12.1	126.0
Sakhalin	1995	7.6	53.0	142.6
Chili	1995	7.3	-24.1	-70.7
Solomon Islands	1995	7.8	-5.5	153.6
Ecuador	1995	7.0	-2.5	-77.5

Mexico	1995	7.3	19.3	-104.8
Egypt	1995	7.3	29.0	34.7
Indonesia	1996	7.7	0.7	119.9
Indonesia	1996	8.1	-0.6	136.6
Aleutian Islands	1996	7.6	51.1	-177.4
Peru	1996	7.3	-15.0	-75.3
Pakistan	1997	7.3	29.7	68.1
Iran	1997	7.3	33.5	60.0
Tibet	1997	7.9	35.3	86.9
Kamchatka	1997	7.6	54.3	161.9
Antarctic plate	1998	8.0	-62.9	148.6
Taiwan	1998	7.3	22.3	125.5
New Guinea	1998	7.1	-2.5	142.0
Ecuador	1998	7.1	-0.5	-80.4
Indonesia	1998	7.0	-6.9	128.9
Indonesia	1998	7.7	-2.0	125.0
Izmit	1999	7.8	41.0	29.9
Hector Mine	1999	7.4	34.7	-116.2
Tonga Islands	2000	7.2	-16.9	-174.2
Vanuatu Islands	2000	7.1	-19.5	173.8
Japan	2000	7.6	22.3	143.7
Argentina	2000	7.0	-28.3	-62.9
Sulawesi	2000	7.6	-1.1	123.5
Argentina	2000	7.2	-23.5	-66.4
Indonesia	2000	7.9	-4.7	102.0
Indian Ocean	2000	7.4	28.8	139.5
Bonin Islands	2000	7.4	28.8	139.5
Vanuatu Islands	2000	7.0	-15.4	166.9
New Ireland, P.N.G	2000	7.0	-4.7	153.9
New Ireland, P.N.G	2000	8.0	-3.9	152.1
New Ireland, P.N.G	2000	7.8	-5.2	153.1
New Ireland, P.N.G	2000	7.6	-5.4	151.7
Turkmenistan	2000	7.0	39.5	54.7